

# Robust MCMC Sampling with Non-Gaussian and Hierarchical Priors in High Dimensions

Victor Chen<sup>1</sup> | Matthew M. Dunlop<sup>1</sup> |  
Omiros Papaspiliopoulos<sup>2</sup> | Andrew M. Stuart<sup>1</sup>

<sup>1</sup>California Institute of Technology,  
Pasadena, CA, USA

<sup>2</sup>ICREA and Universitat Pompeu Fabra,  
Barcelona, Spain

## Contact information

vlchen@caltech.edu  
mdunlop@caltech.edu  
omiros.papaspiliopoulos@upf.edu  
astuart@caltech.edu

## Funding information

MMD and AMS are supported by AFOSR  
Grant FA9550-17-1-0185 and ONR Grant  
N00014-17-1-2079.

A key problem in inference for high dimensional unknowns is the design of sampling algorithms whose performance scales favorably with the dimension of the unknown. A typical setting in which these problems arise is the area of Bayesian inverse problems. In such problems, which include graph-based learning, nonparametric regression and PDE-based inversion, the unknown can be viewed as an infinite-dimensional parameter (such as a function) that has been discretised. This results in a high-dimensional space for inference. Here we study robustness of an MCMC algorithm for posterior inference; this refers to MCMC convergence rates that do not deteriorate as the discretisation becomes finer. When a Gaussian prior is employed there is a known methodology for the design of robust MCMC samplers. However, one often requires more flexibility than a Gaussian prior can provide: hierarchical models are used to enable inference of certain parameters underlying a Gaussian prior; or non-Gaussian priors, such as Besov, are employed to induce sparse MAP estimators; or deep Gaussian priors are used to represent other non-Gaussian phenomena; and finally piecewise constant functions, which are necessarily non-Gaussian, are required for classification problems. The purpose of this article is to show that the simulation technology available for Gaussian priors can be exported to such non-Gaussian priors. The underlying methodology is based on a white noise representation of the unknown function. This is exploited both for robust posterior sampling and for joint inference of the function and parameters involved in the specification of its prior, in which case our framework borrows strength from the well-developed non-centred methodology for Bayesian hierarchical models. The desired robustness of the proposed sampling algorithms is supported by some theory and by extensive numerical evidence from several challenging problems.

## 1 | INTRODUCTION

### 1.1 | Overview

Many problems in statistics and the physical sciences concern the recovery of a latent state given a set of, often indirect, observations. These are examples of inverse problems, in many of which the latent state is infinite-dimensional, such as a function. In others the latent state is so high-dimensional that it can be approximated by an infinite-dimensional object. An example of this setting, which we consider in this article, is graph-based learning: in many settings the large graph may be approximated by a graphon limit or by a differential or integral operator; see [1, 2, 3] and the references therein. Therefore a common mathematical framework for formulating and solving such inverse problems is to consider

them as genuinely infinite-dimensional problems that are discretised to obtain finite, but high, dimensional problems for simulations and inference.

Our focus is Bayesian inference and the use of MCMC to probe the discretised posterior distribution. In many settings it is then important to ensure that the performance of the chosen algorithm, measured for example by its rate of convergence, does not deteriorate as the discretisation of the model becomes finer. In simple terms, the number of samples needed to approximate a given posterior quantity at a specified accuracy should not grow as the discretisation gets finer. Practically, in Metropolis-Hastings algorithms, failing to meet this design criterion typically manifests itself as having to scale the proposed step for the discretised latent state by smaller and smaller constants, as the discretisation gets finer, in order to maintain the same acceptance probability. It is known that naïve application of Metropolis-Hastings algorithms in Bayesian inverse problems will suffer from the deterioration described above; see [4] and references therein for example. The work in this article builds upon developments during the last decade that have established that under Gaussian priors Metropolis-Hastings algorithms can be defined so that their performance does not deteriorate with the size of the discretisation; this is achieved by ensuring that they are well-defined even in the infinite-dimensional limit. Such algorithms enjoy dimension-independent convergence rates, provably in some cases, and empirically verified in others; see [4] for a review upto 2013 and [5, 6, 7, 8] for recent related work. For concreteness in this article we focus primarily on pCN (Algorithm 1) but the philosophy is easily generalised to other, more advanced, methods as one set of numerical experiments will show. Figure 1 illustrates the deterioration of the random walk Metropolis (RWM) algorithm together with the robustness of our proposed algorithm, the whitened pCN, as the discretisation of the unknown (of the order  $1/N$ ) becomes finer. In the figure  $\beta$  controls the proposed jump size and shows that for any choice of  $\beta$ , and for the three different RWM proposal distributions, the acceptance probability of the algorithm decreases as discretisation becomes finer. For the whitened pCN algorithm, however, we obtain a dimension-independent scaling where the acceptance probability is practically the same for all discretisation levels, because it has a non-trivial limit when infinitesimally resolved. The results correspond to a regression analysis, as in Example 1.1, with (non-Gaussian) Besov priors; details may be found in Section 3.3.

This article proposes a generic methodology for robust MCMC sampling in Bayesian inverse problems with non-Gaussian priors and hierarchical conditionally Gaussian priors. Non-Gaussian priors arise naturally in a number of different applications; for example Besov priors are shown to be important in the construction of Bayesian MAP estimators that penalize total variation, e.g., [9]; the use of  $\alpha$ -stable priors for Bayesian inversion is discussed in [10, 11]. In hierarchical priors the motivation is to learn from the data properties of the latent variable which are not known a priori, such as smoothness of a function; [12] describe an asymptotic theory justifying the adoption of such approaches in the setting of linear inverse problems for functions.

The approach we adopt in this paper is to represent non-Gaussian priors as the image of Gaussian white noise under a nonlinear transformation; in the hierarchical setting we introduce a Gaussian white noise latent state with scalar hyperparameters and represent the original latent state via a linear, hyperparameter dependent, transformation of the white noise latent state. With respect to this unknown white noise one may then apply the technology available for robust sampling with Gaussian priors, leading to Algorithm 2, which we call whitened pCN (wpCN). In the hierarchical context this sampling may be part of a Metropolis-within-Gibbs algorithm which alternately samples the latent white noise variable and the hyper-parameters, leading to Algorithm 3. In hierarchical models the different nature and dimension of latent states and hyper-parameters makes such Metropolis-within-Gibbs algorithms appealing. However, the choice of latent state is key: it is known that for high-dimensional latent states Metropolis-within-Gibbs can be very inefficient when there is high prior dependence between parameters and latent states. In the context of Bayesian inverse problems it has been empirically observed and theoretically established that, as the discretisation becomes finer, the update moves become smaller, and the algorithm is unable to move from its initial conditions in the infinite-

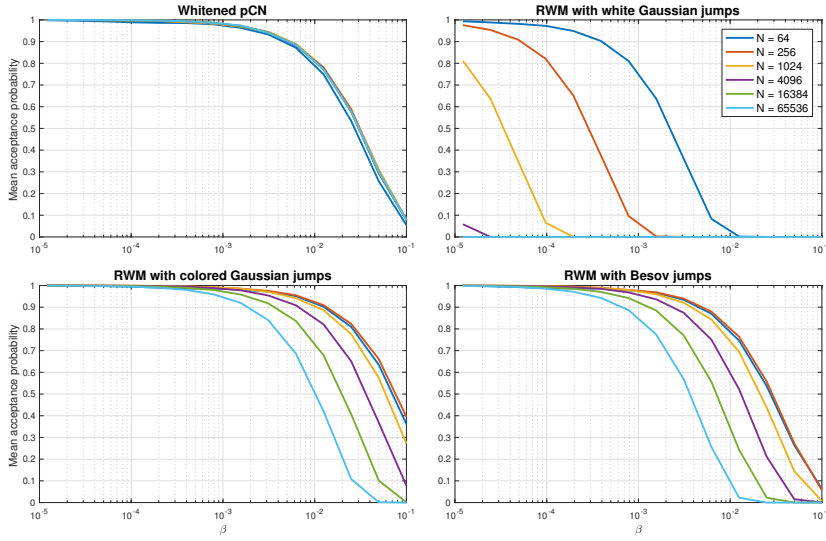


**FIGURE 1** Expected acceptance probability versus jump size  $\beta$  for the whitened pCN algorithm and three random walk Metropolis algorithms. Curves are shown for different state space dimensions  $N$ . Details of the different algorithms can be found in Section 3.3.

dimensional limit, a manifestation of lack of robust sampling. For a generic description of this phenomenon in Bayesian hierarchical models see the review [13] where a non-centred methodology for robust MCMC sampling of latent states and parameters is proposed, and historical development of the subject is given; a recent analysis in the context of linear inverse problems may be found in [14]. The non-centred methodology is based on a transformation of the latent states such that they are a priori independent of the parameters; Metropolis-within-Gibbs is applied on the transformed posterior. The white noise representation of the latent states is precisely one such transformation. Therefore, the computational paradigm we promote in this article unifies two disparate themes of current high interest in Bayesian inference: the use of transformations from non-Gaussians to Gaussians as introduced within the randomise-then-optimize methodology in [15]; and the use of non-centred parameterisations for hierarchical sampling. The appeal of our approach is that it is applicable to a wide variety of problems without needing to design problem-specific mechanisms, and by working exclusively with Gaussians we enable adoption of the many optimised and fast computational tools specific to this setting.

The structure of the paper is as follows. Section 2 considers Gaussian priors, recalls the pCN algorithm for robust sampling in this framework, and describes various different ways of representing Gaussian white noise, all of which are useful in implementing the algorithms which follow. Section 3 introduces the whitened pCN for robust sampling with non-Gaussian priors and demonstrates the success of the approach in some illustrative examples. Section 4 considers hierarchical models where parameters that define the priors in Section 2 are assigned prior distributions of their own; non-centred reparameterisations of such models and robust MCMC samplers for joint inference of latent states and parameters are introduced and the success of the methods in some canonical examples is demonstrated. Section 5 treats the flagship application in this paper which is based on graph-based semi-supervised classification. The remainder of this section outlines the Bayesian inverse problem framework, including our canonical examples, and introduces a notation for the whitening transformations that underpin the remainder of the paper.

## 1.2 | Motivating Bayesian Inverse Problems

The generic structure of a Bayesian inverse problem is that we have data  $y$  assumed to arise from a model  $G$  via

$$y = G(u; \eta) \quad (1)$$

where  $\eta$  is a realisation of some random noise, and we wish to recover the state  $u$ . This problem is typically ill-posed, meaning that the data contains little or no signal, relative to noise, for parts of the state  $u$ , and some type of regularisation is needed to obtain a useful inversion. In the Bayesian approach this is achieved by a prior distribution  $\mu_0$  on  $u$ . The data model (1) leads to the likelihood

$$\mathbb{P}(y|u) = \exp(-\Phi(u; y))$$

of  $y$  given  $u$ , which is combined with  $\mu_0$  using Bayes' theorem, to produce the posterior distribution  $\mu^y$ :

$$\mu^y(du) \propto \exp(-\Phi(u; y))\mu_0(dy).$$

Statistical properties of  $u$  under the posterior distribution can then be estimated from samples from  $\mu^y$ . We give three examples that will be used throughout the paper, when formulated as Bayesian inverse problems, to showcase the success of the methodology we advocate in this article.

**Example 1.1: Regression** We consider the problem of recovering function  $u(x)$  defined on a bounded set  $D \subset \mathbb{R}^d$  from a set of noisily observed linear functionals  $\ell_j(u)$ ; for example point evaluations  $\ell_j(u) = u(x_j)$ . We may place a prior on function  $u$  and use the noise model to define a likelihood and hence a posterior. Formulation of regression problems as inverse problems goes back at least to [16]. ■

**Example 1.2: Graph-based semi-supervised Classification** Consider the problem of dividing a set of  $n$  data points into  $k$  classes, denoted  $\{1, \dots, k\}$ , based on the distribution of the data points and class labels on a subset of these points. More specifically, let  $D = \{x_j\}_{j \in Z} \subset \mathbb{R}^d$  denote a set of data points, and let  $Z' \subset Z$  denote a set of indices of data points for which we have labels  $y_j \in \{1, \dots, k\}$ . The problem is to find a function  $u : D \rightarrow \{1, \dots, k\}$  such that  $u(x_j) = y_j$  for all (or most)  $j \in Z'$ . Many solutions to this under-determined problem exist, and Bayesian regularisation can be used to discriminate between them. The data points  $x_j$  may be identified with graph nodes  $Z$ , and used as prior information on a real-valued latent function over the nodes which implicitly categorises them. The labels define a likelihood and inference may be performed on this latent function. See [17] for a recent work where this type of semi-supervised learning problem is cast as a Bayesian inverse problem. ■

**Example 1.3: PDE-based Inversion** Consider the problem of inferring subsurface permeability from a finite number of noisy pressure head measurements, modelling the forward map with the steady state Darcy equation. More specifically, given a domain of interest  $D \subset \mathbb{R}^d$ , let  $p$  solve the PDE

$$\begin{cases} -\nabla \cdot (u \nabla p) = f & x \in D \\ p = 0 & x \in \partial D. \end{cases}$$

The data  $y$  is given by a finite set of linear functional of  $p$  (such as pointwise measurements), perturbed by noise, and the problem is to recover the coefficient  $u$  (permeability) on the whole of  $D$  from these measurements. Again there will

be many choices of  $u$  for which the resulting measurements will approximately agree with the data – selection of an appropriate coefficient will require prior knowledge of the subsurface, such as presence of different types of rock. A commonly occurring prior model is that the permeability is piecewise constant, with unknown interfaces between known constant values. The problem is one of “classifying” different points in space according to which permeability “category” (value) is taken at that point. For such problems there is an intimate relationship with graph-based classification from the previous example; we will exploit this connection. ■

### 1.3 | Whitening Transformations

We assume that the unknown  $u$ , about which we wish to perform Bayesian inference, lies in a measurable space  $\Xi$ . Let  $X$  be another measurable space, and  $T : \Xi \rightarrow X$  a measurable map. Given a measure  $\nu$  on  $\Xi$ , the *pushforward* measure  $T^\# \nu$  is the measure on  $X$  defined by  $(T^\# \nu)(A) = \nu(T^{-1}(A))$  for each measurable  $A \subseteq X$ . It can be easily verified that if  $\nu$  is a probability measure then so is  $T^\# \nu$ , and  $\xi \sim \nu$  implies that  $T(\xi) \sim T^\# \nu$ . The simple idea we explore in this article is that if  $\mu$  is a probability measure on a space  $X$  and can be expressed as the pushforward of a probability measure  $\nu$  on a different space  $\Xi$ , then we can sample  $\mu$  by sampling  $\nu$  and transforming the samples using  $T$ . We introduce the transformation  $T$  via the prior: for choices of  $\mu_0$  among common priors in Bayesian inverse problems and  $\nu_0$  the Gaussian white noise process we identify the transformation  $T$  that makes  $\mu_0$  the pushforward of  $\nu_0$ ; more formally we refer to the triplet  $(\Xi, \nu_0, T)$  as a white noise representation of  $\mu_0$ .

## 2 | GAUSSIAN PRIORS

### 2.1 | Robust Algorithms

Our primary focus throughout this article is on the preconditioned Crank-Nicolson (pCN) for Bayesian inverse problems. The basic form applies when the prior  $\mu_0$  is the centred Gaussian  $N(0, C)$  and it is presented in Algorithm 1.

---

#### Algorithm 1 Preconditioned Crank-Nicolson (pCN)

---

- 1: Fix  $\beta \in (0, 1]$ . Choose initial state  $u^{(0)} \in X$  and set  $k = 0$ .
- 2: **for**  $k = 0, \dots, K - 1$  **do**
- 3:   Propose  $\hat{u}^{(k)} = (1 - \beta^2)^{\frac{1}{2}} u^{(k)} + \beta \zeta^{(k)}$ ,    $\zeta^{(k)} \sim N(0, C)$ .
- 4:   Set  $u^{(k+1)} = \hat{u}^{(k)}$  with probability

$$\min \left\{ 1, \exp \left( \Phi(u^{(k)}; y) - \Phi(\hat{u}^{(k)}; y) \right) \right\}$$

or else set  $u^{(k+1)} = u^{(k)}$ .

5: **end for**

6: **return**  $\{u^{(k)}\}_{k=0}^K$ .

---

Most of this paper will be based on generalizing the pCN Algorithm 1 to apply to non-Gaussian priors and to hierarchical conditionally Gaussian priors. However other dimension robust algorithms can be used in place of the pCN algorithm, for improved efficiency. The reader will readily appreciate that the basic building block of the pCN method may be replaced by any other dimension robust algorithm.

## 2.2 | White Noise Representation of Gaussian Priors

In this subsection we show how the pCN Algorithm 1 may be reformulated in terms of a white noise representation, in the simple setting of Gaussian priors. To be concrete we consider the case of Gaussian prior probability measure  $\mu_0$  on a separable Hilbert space  $X$  of continuous real-valued functions defined on bounded open  $D \subseteq \mathbb{R}^d$ . Measure  $\mu_0$  can then be characterised by its mean function  $m : D \rightarrow \mathbb{R}$  and covariance function  $c : D \times D \rightarrow \mathbb{R}$ , and is then commonly written as

$$\mu_0 = \text{GP}(m(x), c(x, x')).$$

The covariance function can be used to define a symmetric positive semi-definite covariance operator  $C : X \rightarrow X$  by

$$(C\varphi)(x) = \int_D c(x, x')\varphi(x') dx' \quad (2)$$

for any  $\varphi \in X, x \in D$ ; we can then alternatively write  $\mu_0 = N(m, C)$ . The operator  $C$  is necessarily compact (in fact, it is trace class) and its inverse, the precision operator  $\mathcal{L} : D(\mathcal{L}) \rightarrow X$ , has domain  $D(\mathcal{L})$  which is dense in  $X$ . White noise on  $X$  is defined as the centred Gaussian measure with covariance operator given by the identity. In infinite dimensions the identity is not trace class, and as a consequence samples of white noise almost surely do not take space in the Hilbert space  $X$  itself; they live in weighted  $\ell_2$  spaces which contain  $X$ , see for example the review in [18]. We now give three examples of white noise representations of  $\mu_0$ .

### 2.2.1 | Cholesky Factorisation of Covariance Matrix

Consider the centred Gaussian process  $\mu_0 = \text{GP}(0, c(x, x'))$  restricted to a set of  $n$  points  $D_n = \{x_j\}_{j=1}^n \subset D$ . Define matrix  $C_n \in \mathbb{R}^{n \times n}$  by  $(C_n)_{ij} = c(x_i, x_j)$  and denote by  $C_n = Q_n Q_n^*$  the Cholesky decomposition of  $C_n$ . If

$$\Xi = \mathbb{R}^n, \quad v_0 = N(0, I), \quad T(\xi) = Q_n \xi$$

then  $(\Xi, v_0, T)$  is a white noise representation of  $\mu_0$  restricted to  $D_n$ . The decomposition requires  $O(n^3)$  operations unless the matrix  $C_n$  has specific types of sparsity, hence obtaining this white noise representation may be infeasible when  $n$  is very large. See [19] for an overview.

### 2.2.2 | Factorisations of Precision Operator

Consider the Gaussian measure  $\mu_0 = N(0, C)$  on  $X = L^2(D; \mathbb{R})$ , where the inverse covariance operator,  $\mathcal{L}$ , is some densely defined differential operator  $\mathcal{L}$  on  $X$ . The locality of the differential operator is a form of infinite dimensional sparsity, and certain finite dimensional approximations of the operator, e.g. finite elements or finite difference methods, result in sparse matrices. In fact, there is a close link between Gaussian Markov random fields and Gaussian processes with differential precision operators. Suppose further that  $\mathcal{L}$  may be factorised as  $\mathcal{L} = \mathcal{A}^* \mathcal{A}$ , where  $\mathcal{A}$  is itself a differential operator. Then samples  $u \sim \mu_0$  can be generated by solving the stochastic PDE (SPDE)

$$\mathcal{A}u = \xi, \quad (3)$$

which provides the white noise representation by taking  $T$  to be the solution mapping  $\xi \mapsto u$ . Although  $\Xi$  will be larger than  $X$  (a weighted  $\ell_2$  space closely related to, or equivalent to, a Sobolev space with negative exponent) its image under  $T$  will be contained in  $X$  as  $T$  is a smoothing operator. [20] systematise the above construction when the Gaussian process is specified via taking its covariance function to be in the Matérn family. When a sparsity-preserving discretisation is applied to obtain a matrix  $A_n$  approximating  $\mathcal{A}$ , so that  $L_n^* L_n$  approximates  $\mathcal{L}$ , the white noise representation of the finite-dimensional approximation is given by  $(\mathbb{R}^n, N(0, I), T(\xi) = A_n^{-1} \xi)$ . Fast PDE solvers can be utilised to evaluate  $T$  efficiently. In contrast to the previous subsection this is based on a factorisation of the precision as opposed to the covariance matrix. Simulation and computations for finite-dimensional Gaussian Markov random fields based on Cholesky factorisation of the precision matrix was systematised in [21].

### 2.2.3 | Karhunen-Loève Expansion.

The properties of  $C$  mean that it admits a complete orthonormal basis of eigenvectors  $\{\varphi_j\}_{j \geq 1}$  for  $X$  with corresponding non-negative and summable eigenvalues  $\{\lambda_j\}_{j \geq 1}$ ; this gives rise to natural spectral methods where functions in  $X$  are represented via expansions in this basis, and approximations may be made by truncating such expansions. As a consequence of the Karhunen-Loève theorem  $\mu_0 = N(0, C)$  is equal to the law of the random variable  $u$  defined by

$$u = \sum_{j=1}^{\infty} \sqrt{\lambda_j} \xi_j \varphi_j, \quad \xi_j \stackrel{\text{i.i.d.}}{\sim} N(0, 1).$$

Thus, the white noise representation of  $\mu_0$  is obtained as  $\Xi = \mathbb{R}^{\infty}$ ,  $v_0 = N(0, 1)^{\infty}$ , and

$$T(\xi) := \sum_{j=1}^{\infty} \sqrt{\lambda_j} \xi_j \varphi_j.$$

This series-based construction and white noise representation will be used later for certain non-Gaussian priors. Of course, the  $\varphi_j$  are eigenfunctions of  $\mathcal{L}$  and  $\lambda_j^{-1}$  the corresponding eigenvalues, hence this method is essentially a special case of the methods based on factorising the precision operator, wherein a spectral method is used for the evaluation of  $T$ .

### 2.2.4 | Example: Whittle-Matérn Covariance

This example serves to illustrate all of the above, and will also play a role as the canonical example of conditionally Gaussian hierarchical priors. We start by introducing the process through its covariance function

$$c(x, x') = \sigma^2 \frac{2^{1-\beta}}{\Gamma(\beta)} (\tau |x - x'|)^{\beta} K_{\beta}(\tau |x - x'|), \quad x, x' \in \mathbb{R}^d,$$

where  $\sigma, \tau, \beta > 0$  are scalar parameters representing standard deviation, inverse length-scale and regularity respectively. Here  $\Gamma$  is the gamma function and  $K_{\beta}$  is the modified Bessel function of the second kind of order  $\beta$ . If  $\mu_0 = \text{GP}(0, c(x, x'))$  and  $u \sim \mu_0$ , then almost-surely  $u$  has  $s$  Sobolev and Hölder derivatives for any  $s < \beta$ . This defines a Gaussian over the whole of  $\mathbb{R}^d$ , but the covariance can be restricted to a bounded open subset  $D$ .

The Cholesky factorisation of the covariance matrix can be used to obtain a white noise representation if we restrict to a finite subset of points  $\{x_j\}_{j=1}^n$ . But we cannot obtain a white noise representation for the whole process using this

method. We can, however, obtain a white noise representation by using a factorisation of the precision operator which, for this covariance on the whole of  $\mathbb{R}^d$ , has the form

$$\mathcal{L} = \sigma^{-2} \tau^{-2\beta} q(\beta)^{-1} (\tau^2 I - \Delta)^{(\beta+d/2)}, \quad q(\beta) = \frac{2^d \pi^{d/2} \Gamma(\beta + d/2)}{\Gamma(\beta)}, \quad (4)$$

where  $\Delta$  is the second-order differential Laplacian operator. In [20] it is noted that the square root of  $\mathcal{L}$  is

$$\mathcal{A} = \sigma^{-1} \tau^{-\beta} q(\beta)^{-1/2} (\tau^2 I - \Delta)^{(\beta+d/2)/2}. \quad (5)$$

We thus have a factorisation of the precision, and this may be used to define a white noise representation of the Gaussian. The method can be implemented on a finite domain by means of finite difference or finite element methods when  $(\beta + d/2)/2$  is an integer, and by choosing appropriate boundary conditions on a finite domain  $D \subset \mathbb{R}^d$ . Note, however, that the the boundary conditions may modify the covariance structure near the boundary.<sup>1</sup> When the exponent of the differential operator in  $\mathcal{A}$  is not an integer, its action may be defined through the Fourier transform  $\mathcal{F}$ , i.e.

$$\mathcal{F}(\mathcal{A}u)(\omega) = \sigma^{-1} \tau^{-\beta} q(\beta)^{-1/2} (\tau^2 + |\omega|^2)^{(\beta+d/2)/2}.$$

This leads to spectral methods and the Karhunen-Loève white noise representation. Suppose  $D \subset \mathbb{R}^d$  is a bounded rectangle, and homogeneous Neumann or Dirichlet boundary condition are applied. Then the eigenvectors of  $\mathcal{A}$  are known analytically, and given by Fourier basis functions. For example, if  $D = (0, 1)$  and homogeneous Neumann boundary conditions are assumed, we have

$$C\varphi_j = \lambda_j \varphi_j, \quad \varphi_j(x) = \sqrt{2} \cos(j\pi x), \quad \lambda_j = \sigma^2 \tau^\beta q(\beta) (\tau^2 + \pi^2 j^2)^{-\beta-d/2}.$$

The Karhunen-Loève expansion may then be efficiently implemented numerically using the fast Fourier transform.

### 3 | NON-GAUSSIAN PRIORS

Assume that  $\mu_0$  admits a white noise representation  $(\Xi, v_0, T)$ . If we define

$$\nu^y(d\xi) \propto \exp(-\Phi(T(\xi); y)) v_0(dy)$$

then the fact that  $\mu_0 = T^\# v_0$  implies that  $\mu^y = T^\# \nu^y$ . In the case of Gaussian  $\mu_0$  we have given examples of such transformations  $T$ , and in subsection 3.2 we show a range of non-Gaussian priors which can be pre-whitened. In particular we consider uniform, Besov, stable and level set priors.

<sup>1</sup>A simple method to ameliorate these effects is to perform sampling on a larger domain  $D^* \supset D$  so that samples restricted to  $D$  are approximately stationary. More complex methods have also been considered, for example by optimal choice of a constant Robin boundary condition, as in [22], or of a variable Robin boundary condition combined with variance normalisation, as in [23].



### 3.1 | Robust Algorithms

We may use the pCN algorithm to sample the posterior  $\nu^y$ , and then evaluate  $T$  at these samples to produce samples from  $\mu^y$ . This method is presented in Algorithm 2.

---

**Algorithm 2** Whitened Preconditioned Crank-Nicolson (wpCN)
 

---

- 1: Fix  $\beta \in (0, 1]$ . Choose initial state  $\xi^{(0)} \in \Xi$  and set  $k = 0$ .
- 2: **for**  $k = 0, \dots, K - 1$  **do**
- 3:   Propose  $\hat{\xi}^{(k)} = (1 - \beta^2)^{\frac{1}{2}} \xi^{(k)} + \beta \zeta^{(k)}$ ,  $\zeta^{(k)} \sim \mathcal{N}(0, I)$ .
- 4:   Set  $\xi^{(k+1)} = \hat{\xi}^{(k)}$  with probability

$$\min \left\{ 1, \exp \left( \Phi(T(\xi^{(k)}); y) - \Phi(T(\hat{\xi}^{(k)}); y) \right) \right\}$$

or else set  $\xi^{(k+1)} = \xi^{(k)}$ .

- 5: **end for**
  - 6: **return**  $\{T(\xi^{(k)})\}_{k=0}^K$ .
- 

Note that if  $T$  is differentiable we can use a geometric method, which involves derivatives of the likelihood, in place of pCN;  $T$  is differentiable for the uniform, Besov and stable priors described below, and there we can calculate its derivative explicitly. Note however that  $T$  is not differentiable for the level set map.

### 3.2 | White Noise Representation of Non-Gaussian Priors

We now describe a number of families of non-Gaussian distributions, and the construction of corresponding white noise representations. We focus on those which are defined through series expansions – the construction of these priors is inspired by the Karhunen-Loève expansion for Gaussian processes, except the basis does not necessarily correspond to the eigenbasis of a given operator, and the randomness introduced to each mode is not necessarily Gaussian. Another approach to define families of non-Gaussian distributions on function space is through the SPDE (3) when the white noise is non-Gaussian; we do not consider this approach explicitly, though the ideas discussed can be applied in such cases too.

In what follows, the prior  $\mu_0$  will be given by the law of the  $X$ -valued random variable defined by

$$u = m + \sum_{j=1}^{\infty} \rho_j \zeta_j \varphi_j, \tag{6}$$

where  $\rho = \{\rho_j\}_{j \geq 1}$  is a deterministic real-valued sequence,  $\zeta = \{\zeta_j\}_{j \geq 1}$  is a random real-valued sequence,  $\{\varphi_j\}_{j \geq 1}$  is a deterministic  $X$ -valued sequence, and  $m \in X$ .

For each of the classes of priors considered the construction of a white noise representation is common:

1. Write down a method for sampling  $\zeta_j$ .
2. Using an inverse CDF type method, rewrite this sampling method in terms of a (possibly multivariate) Gaussian random variable. This defines a deterministic mapping  $\Lambda$  taking a Gaussian random variable  $\xi_j$  to a sample  $\zeta_j$ .
3. Define  $T$ , mapping  $\{\xi_j\}_{j \geq 1}$  to  $u$ , by replacing  $\zeta_j$  with  $\Lambda(\xi_j)$  in (6), and define  $\nu_0$  to be the joint distribution of the Gaussians  $\{\xi_j\}_{j \geq 1}$ .

The above construction may be applied to other classes of series-based priors not considered here, for example the infinitely divisible priors considered in [24]. The construction of the distributions considered in this section involves selection of hyperparameters, which may be treated hierarchically similarly to the Gaussian case treated in Section 4. The idea of transforming non-Gaussians into Gaussians was systematically exploited in the context of randomise-then-optimize algorithms and our work builds on this; see [15].

### 3.2.1 | Uniform Priors

Here we work with the uniform priors; see [18] for a historical review. Let  $D \subseteq \mathbb{R}^d$  be a bounded open subset, let  $\{\varphi_j\}_{j \geq 1} \subseteq L^\infty(D)$ , and define  $X$  to be the closure of the linear span of this sequence in  $L^\infty(D)$ . Assume that  $\rho \in \ell^1$ ,  $m \in X$ , and let  $\zeta_j \stackrel{\text{i.i.d.}}{\sim} \mathcal{U}(-1, 1)$ .

We construct a white noise representation of  $\mu_0$ . Let  $F$  denote the cumulative distribution function of a standard normal random variable, define  $\Lambda(z) = 2F(z) - 1$  and let  $\xi \sim \mathcal{N}(0, 1)$  then it is elementary that  $\Lambda(\xi) \sim \mathcal{U}(-1, 1)$ . Thus, define the map  $T : \mathbb{R}^\infty \rightarrow X$  by

$$T(\xi) = m + \sum_{j=1}^{\infty} \gamma_j \Lambda(\xi_j) \varphi_j,$$

and let  $v_0 = \mathcal{N}(0, I)$ . Then the above calculation shows that the triple  $(\mathbb{R}^\infty, v_0, T)$  forms a white noise representation of  $\mu_0$ .

### 3.2.2 | Besov Priors

Besov priors were introduced in [9] and analysed further in [25]. They generalise Gaussian priors by allowing for control over the weight of their tails. Let  $D \subseteq \mathbb{R}^d$  be a bounded open domain, and define  $X = L^2(D)$ . Let  $\{\varphi_j\}_{j \geq 1}$  be a basis for  $X$ , and choose  $m \in X$ . Given  $s > 0$  and  $q \geq 1$ , define the Banach space  $X^{s,q} \subseteq X$  through the norm

$$\|u\|_{X^{s,q}}^q = \sum_{j=1}^{\infty} j^{sq/d+q/2-1} |u_j|^q \quad \text{where} \quad u = \sum_{j=1}^{\infty} u_j \varphi_j.$$

If  $D = \mathbb{T}^d$  is the torus, and  $\{\varphi_j\}_{j=1}^{\infty}$  is chosen to be an  $r$ -regular wavelet basis for  $X$  with  $r > s$ , then  $X^{s,q}$  is the Besov space  $B_{q,q}^s$  [9].

The series based construction (6) can be used to produce probability measures with strong links to the above spaces. Given  $s, q$  as above and  $\kappa > 0$ , define the sequence  $\{\rho_j\}_{j \geq 1}$  by

$$\rho_j = \kappa^{-\frac{1}{q}} j^{-(\frac{s}{d} + \frac{1}{2} - \frac{1}{q})}.$$

Let  $\{\zeta_j\}_{j \geq 1}$  be an i.i.d. sequence of draws from the distribution defined via the density

$$\pi_q(x) \propto \exp\left(-\frac{1}{2}|x|^q\right),$$

and let  $m \in X$ . The measure  $\mu_0$  is a  $(\kappa, B_{q,q}^s)$  measure in the sense of [25] and, when  $m = 0$ , it formally has Lebesgue density proportional to  $\exp\left(-\frac{\kappa}{2}\|u\|_{X^{s,q}}^q\right)$ . The cases  $q = 1$  are of particular interest since they allow for discretisation

invariant edge-preserving Bayesian inversion; this is in contrast to total variation priors which are often used in classical inversion for edge-preservation as in [9]. MAP estimation using these priors is well-defined and corresponds to Besov regularised optimisation as in [26]. These methods may be viewed as Bayesian and infinite-dimensional analogues of the lasso.

We construct a white noise representation of  $\mu_0$ . In order to do this, we first write down a method for sampling the scalar distribution  $\pi_q$ . We use the method of [27]: a sample  $\zeta \sim \pi_q$  can be produced as

$$\zeta = 2^{1/q} B \cdot G^{1/q}, \quad B \sim \text{Bernoulli}(1/2), \quad G \sim \text{Gamma}(1/q, 1)$$

where  $B$  and  $G$  are independent. We claim that a single standard normal random variable  $\xi \sim N(0, 1)$  may be transformed into the pair  $B, G$  above. Observe first that  $\text{sgn}(\xi)$  and  $|\xi|$  are independent, and  $\text{sgn}(\xi) \sim \text{Bernoulli}(1/2)$ . To transform  $|\xi|$  into  $G$ , we first note that the cumulative distribution function of  $|\xi|$  is given by  $2F(z) - 1$ , where as earlier in the paper  $F$  denotes the standard Gaussian distribution function. Hence  $2F(|\xi|) - 1 \sim U(0, 1)$ . Using the inverse CDF method, this can in turn be transformed into the appropriate gamma distribution:

$$\gamma_{1/q}^{-1}(2F(|\xi|) - 1) \sim \text{Gamma}(1/q, 1),$$

where  $\gamma_{1/q}$  is the normalised lower incomplete gamma function:

$$\gamma_{1/q}(z) = \frac{1}{\Gamma(1/q)} \int_0^z t^{1/q-1} e^{-t} dt.$$

We therefore define the map  $\Lambda : \mathbb{R} \rightarrow \mathbb{R}$  by

$$\Lambda(\xi) = 2^{1/q} \text{sgn}(\xi) \left( \gamma_{1/q}^{-1}(2F(|\xi|) - 1) \right)^{1/q}$$

and the map  $T : \mathbb{R}^\infty \rightarrow X$  by

$$T(\xi) = \sum_{j=1}^{\infty} \rho_j \Lambda(\xi_j) \varphi_j.$$

Then, as for the uniform priors, defining  $v_0 = N(0, I)$  we see that  $(\mathbb{R}^\infty, v_0, T)$  gives a white noise representation of  $\mu_0$ .

**Remark** A similar white noise representation to the above is provided in [15], in the cases where  $q = 1$  and the sum (6) is truncated after a finite number of terms. A randomise-the-optimize approach is used to sample the posterior rather than MCMC, which should extend easily to the cases  $q > 1$  considered here.

### 3.2.3 | Stable Priors

Stable priors are a class of priors that again generalise Gaussian priors, by allowing for control over tail weights and scaling properties. They are introduced and analysed in [11] in the context of Bayesian inversion. Their intersection with Besov distributions is precisely the set of Gaussian distributions, and they arise by assuming that each of the random variables  $\zeta_j$  in (6) is a stable random variable. The set of stable distributions on  $\mathbb{R}$  can be interpreted as the set of distributions that are limits in central limit theorems, and may be defined via their characteristic function. Let  $\alpha \in (0, 2]$ ,  $\beta \in [-1, 1]$ ,  $\gamma \in (0, \infty)$  and  $\delta \in \mathbb{R}$  be scalar parameters, representing stability, skewness, scale and location

respectively. We will say that a real-valued random variable  $\zeta$  has stable distribution  $S(\alpha, \beta, \gamma, \delta)$  if, for each  $t \in \mathbb{R}$ ,

$$\mathbb{E}(e^{-it\zeta}) = \begin{cases} \exp(it\delta - |\gamma t|^\alpha [1 + i\beta \tan(\frac{\pi\alpha}{2}) \operatorname{sgn}(t)(|\gamma t|^{1-\alpha} - 1)]) & \alpha \neq 1 \\ \exp(it\delta - |\gamma t| [1 + i\beta \frac{2}{\pi} \operatorname{sgn}(t) \log(\gamma|t|)]) & \alpha = 1. \end{cases}$$

The Lebesgue density of a  $S(\alpha, \beta, \gamma, \delta)$  distribution is typically not expressible analytically, however it is known these distributions are unimodal and possess  $\lceil \alpha - 1 \rceil$  moments;  $\alpha = 2$  corresponds to the Gaussian distributions, and  $\alpha = 1$  to the Cauchy.

Let  $D \subseteq \mathbb{R}^d$  be a bounded open domain,  $X = L^2(D)$ , and let  $\{\varphi_j\}_{j \geq 1}$  be a normalised basis for  $X$ . Given  $\alpha \in (0, 2]$  and sequences  $\beta = \{\beta_j\} \subseteq [-1, 1]^\infty$ ,  $\gamma = \{\gamma_j\} \subseteq (0, \infty)^\infty$  and  $\delta = \{\delta_j\} \subseteq \mathbb{R}^\infty$ , let the random sequence  $\{\zeta_j\}_{j \geq 1}$  in (6) be defined by

$$\zeta_j \sim S(\alpha, \beta_j, \gamma_j, \delta_j) \quad \text{independent.}$$

Define also  $\rho_j = 1$  for each  $j$ , and let  $m \in X$ .

We construct a white noise representation of  $\mu_0$  using the same technique as for the Besov priors, that is, we take a known sampling method for stable random variables and rewrite it in terms of Gaussians. One difference however is that we will in general require two independent  $N(0, 1)$  random variables to construct a single  $S(\alpha, \beta, \gamma, \delta)$  random variable, doubling the dimension of the state space when implemented numerically. The sampling method we use is the CMS method presented by [28], which is a generalisation of the Box-Muller transform for sampling Gaussian random variables. In this method, a sample  $\zeta \sim S(\alpha, \beta, \gamma, \delta)$  may be produced using a  $U(-\pi/2, \pi/2)$  and an  $\text{Exponential}(1)$  random variable. We define

$$U(\xi) = \pi F(\xi) - \frac{\pi}{2}, \quad W(\xi') = -\log(F(\xi'))$$

so that  $U(\xi), W(\xi')$  have the requisite distributions for  $\xi, \xi' \stackrel{\text{i.i.d.}}{\sim} N(0, 1)$ . Combining the CMS method with similar arguments as used for the Besov prior leads us to define

$$\Lambda(\xi, \xi'; \alpha, \beta, \gamma, \delta) = \begin{cases} \delta + \gamma(1 + \tau^2)^{\frac{1}{2\alpha}} \frac{\sin(\alpha(U(\xi) + \theta))}{\cos(U(\xi))^{1/\alpha}} \left\{ \frac{\cos(U(\xi) - \alpha(U(\xi) + \theta))}{W(\xi')} \right\}^{\frac{1-\alpha}{\alpha}} & \alpha \neq 1 \\ \delta + \tau + \frac{\gamma}{\theta} \left\{ \left( \frac{\pi}{2} + \beta U(\xi) \right) \tan(U(\xi)) - \beta \log \left( \frac{\pi W(\xi') \cos(U(\xi))}{\pi + 2\beta U(\xi)} \right) \right\} & \alpha = 1 \end{cases}$$

where

$$\tau = \begin{cases} -\beta \tan(\frac{\pi\alpha}{2}) & \alpha \neq 1 \\ \frac{2}{\pi} \beta \gamma \log(\gamma) & \alpha = 1, \end{cases} \quad \theta = \begin{cases} \frac{1}{\alpha} \tan^{-1}(-\tau) & \alpha \neq 1 \\ \frac{\pi}{2} & \alpha = 1. \end{cases}$$

It then follows that  $\Lambda(\xi, \xi'; \alpha, \beta, \gamma, \delta) \sim S(\alpha, \beta, \gamma, \delta)$  for  $\xi, \xi' \stackrel{\text{i.i.d.}}{\sim} N(0, 1)$ . Now define the map  $T : \mathbb{R}^\infty \times \mathbb{R}^\infty \rightarrow X$  by

$$T(\xi, \xi') = \sum_{j=1}^{\infty} \Lambda(\xi_j, \xi'_j; \alpha, \beta_j, \gamma_j, \delta_j) \varphi_j,$$

and  $\nu_0 = N(0, I) \times N(0, I)$ . Then  $(\mathbb{R}^\infty \times \mathbb{R}^\infty, \nu_0, T)$  forms a white noise representation of  $\mu_0$ .

### 3.2.4 | Level Set Priors

A large class of inverse problems involve the recovery of a piecewise constant function. This class includes classification problems as in Example 1.3 where the unknown function is a mapping from the set of data points to a discrete set of classes. It also includes PDE-based inversion as in Example 1.3: here the unknown permeability may be approximately piecewise constant, with the different values corresponding to the permeability of different materials. The key part of such inversion is the recovery of the interfaces separating the different classes. Level set methods are a popular choice of methods for inverse interface problems, as they require no prior knowledge or assumption on the topology of the different classes, see [29, 30]. The Bayesian level set and hierarchical Bayesian level set methods were recently introduced in [31] and [32] respectively to allow for uncertainty quantification in inverse interface problems.

The idea of level set methods is to create a piecewise constant field by thresholding a continuous field. Let  $D \subseteq \mathbb{R}^d$  be a bounded open domain, and define  $X = L^\infty(D; \mathbb{R})$ , the space of bounded measurable  $\mathbb{R}$ -valued functions on  $D$ , and  $V = C^0(D; \mathbb{R})$ , the space of bounded continuous  $\mathbb{R}$ -valued functions on  $D$ . Choose classes  $\kappa_1, \dots, \kappa_k \in \mathbb{R}$  and thresholding levels  $c_1 < \dots < c_{k-1} \in \mathbb{R}$ , and define  $S : V \rightarrow X$  by

$$(Sv)(x) = \begin{cases} \kappa_1 & v(x) \leq c_1 \\ \kappa_2 & c_1 < v(x) \leq c_2 \\ \vdots & \\ \kappa_{k-1} & c_{k-2} < v(x) \leq c_{k-1} \\ \kappa_k & c_{k-1} < v(x). \end{cases} \quad (7)$$

Then given any continuous function  $v \in V$ ,  $S(v)$  is a piecewise constant function taking values in the set of classes  $\{\kappa_1, \dots, \kappa_k\}$ . Hence, given a measure  $\lambda_0$  on  $V$  such as those defined in the previous subsections, its pushforward  $\mu_0 = S^\# \lambda_0$  defines a measure that concentrates on piecewise constant functions. To obtain a white noise representation of  $\mu_0$  we first obtain a whitening of  $\lambda_0$ , say  $(\Xi, v_0, T_0)$ , using a method as described in the subsections 2.2 and 3.2, and then  $(\Xi, v_0, T)$ , with  $T = S \circ T_0$  provides a white noise representation of  $\mu_0$ . In our examples in this paper  $\lambda_0$  is always Gaussian.

One restriction of the above method is that there is an ordering of the classes: arbitrary classes cannot share an interface, and so, for example, a triple-junction cannot be formed. Vector level set methods allow one to get around this restriction, in exchange for increasing the dimension of the unknown field. One such method is that of [33], in which we take  $V = C^0(D; \mathbb{R}^k)$ ,  $X = L^\infty(D; \mathbb{R}^k)$  and define  $S : V \rightarrow X$  by

$$(Sv)(x) = e^{r(x; v)}, \quad r(x; v) = \arg \max_{r=1, \dots, k} v_r(x), \quad (8)$$

where  $\{e^r\}_{r=1}^k$  denotes the standard basis for  $\mathbb{R}^k$ .

In regression problems (Example 1.1) for piecewise constant functions the likelihood is found from pointwise observations of  $u = Sv$  subject to additive noise. Thus

$$y_j = S(v(x_j)) + \eta, \quad \eta \sim N(0, \gamma^2 I),$$

for some set of observation points  $\{x_j\}_{j=1}^J \subset D$ . For PDE based inverse problems (Example 1.3) observations are

typically of some nonlinear function  $G(u)$  where  $u = S\nu$  :

$$y_j = G(v(x_j)) + \eta, \quad \eta \sim N(0, \gamma^2 I).$$

For classification problems (Example 1.2), a variant of level set methods for regression is obtained by modelling the noise as additive with respect to  $v$  and not  $u$ , so that

$$y_j = S(v(x_j) + \eta), \quad \eta \sim N(0, \gamma^2 I).$$

For example, if the model (7) is used with two classes  $\kappa_1 = 1, \kappa_2 = -1$ , this leads to the negative log-likelihood<sup>2</sup>

$$\Phi(\nu; y) = - \sum_{j=1}^J \log F(v(x_j)y_j/\gamma)$$

where  $F$  is the standard normal CDF as above.

### 3.3 | Simulation experiments

We first compare wpCN algorithm with three random walk Metropolis (RWM) algorithms on a problem with a Besov prior. The prior is of the form described in subsection 3.2.2, with  $q = 1, s = 3$  and  $d = 2$ , and a Fourier basis is used for the expansion; specifically we take  $m = 0, \rho_j = (k_1^2 + k_2^2)^{-1}$  and  $\varphi_j(x, y) = 2 \cos(k_1 \pi x) \cos(k_2 \pi y)$ , where we have enumerated  $k_1^2 + k_2^2 \asymp j$ . The model is of the type described in Example 1.1 in the case where the forward map corresponds to point evaluations on a uniform grid of 16 points in the domain  $(0, 1)^2$ , and the observations are perturbed by white noise with standard deviation 0.1. The true field is drawn from the prior distribution. The three RWM algorithms differ in the distribution of their proposal jumps. Each RWM proposal is of the form  $u \mapsto u + \beta \zeta$  for some  $\beta > 0$ , and  $\zeta$  is a centred random variable. We consider first the case where  $\zeta \sim N(0, I)$  is Gaussian white noise. We then consider  $\zeta \sim N(0, C)$  where the covariance is defined on the basis  $\{\varphi_j\}$  by  $C\varphi_j = \rho_j^2 \varphi_j$ , so that samples possess the same spectral decay rate as the prior distribution. We finally consider the case where  $\zeta$  is drawn from the prior distribution. Results from this simulation experiment were shown in Figure 1, which clearly shows that for the whitened pCN algorithm these curves are stable under refinement of the discretisation; in contrast for the RWM algorithms the curves shift with changing discretisation and, in particular, the proposal size allowable for given acceptance probability decreases with dimension.

We now demonstrate that the perspective of this paper opens up the possibility of the systematic use of a range of generic methods which improve upon existing tailored to specific models. In particular we compare the methodology presented in [34] for uniform priors. We compare the reflected uniform and Gaussian random walk proposals, referred to as RURWM and RSRWM respectively and derived in [34], with the wpCN method. Additionally, as a Gaussian prior is used for the reparameterised model, we have a variety of dimension robust algorithms available that use likelihood-informed proposals; we therefore also compare with the whitened  $\infty$ -MALA method developed for Gaussian priors in [5], which we refer to as  $\infty$ -wMALA. We study Example 1.1 in the case where the forward map corresponds to convolution with a heat kernel, composed with pointwise evaluation at equally spaced points on the domain  $(0, 1)$ . A uniform prior of the form (6) is used, with  $m = 2, \rho_j = 1/j^2$  and  $\varphi_j(x) = \sqrt{2} \cos(j\pi x)$  for each  $j \geq 1$ . Jump size parameters are chosen such that the acceptance rate is roughly 30% for wpCN, RURWM and RSRWM, and roughly 60% for  $\infty$ -wMALA. The true field is generated on a mesh of  $2^{12}$  points, and observations are corrupted with Gaussian noise with standard deviation such

<sup>2</sup>This likelihood function is sometimes referred to as the probit likelihood function [19].

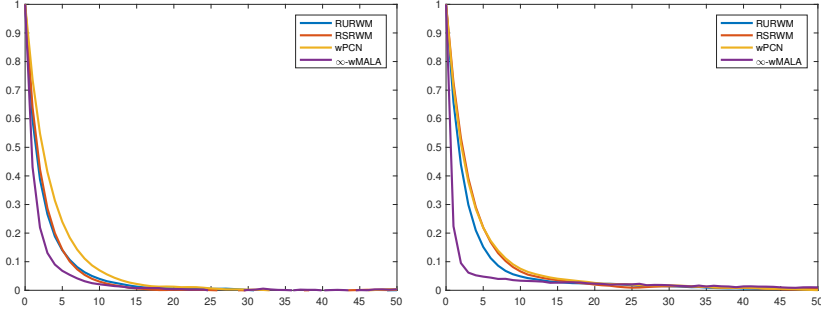


**FIGURE 2** Autocorrelations for the different MCMC chains using the heat equation forward model, with 8 observations (left) and 32 observations (right).

that the average relative error is approximately 4%. Sampling is performed on a mesh of  $2^{10}$  points. Autocorrelations for different numbers of observation points are shown in Figure 2. The results demonstrate that the wpCN and  $\infty$ -wMALA algorithms behave similarly to the existing ad hoc methods derived to be robust for this prior, whilst also holding the potential to generalise to different priors.

## 4 | HIERARCHICAL PRIORS

### 4.1 | Robust Algorithms

Taking into account parameter uncertainty, we now define  $\mu_0$  as a hierarchical prior on  $X \times \Theta$ , disintegrated as  $\mu_0(du, d\theta) = \mu_0(du|\theta)\pi_0(\theta)d\theta$ , with  $\theta$  a vector of parameters that define it and where we assume that the marginal prior distribution on the parameters  $\theta$  admits Lebesgue density  $\pi_0$ . Note the conditional distribution  $\mu_0(du|\theta)$  may concentrate on different subsets of  $X$  for different  $\theta$ , such as sets of fields with a specific regularity. With these ingredients the target posterior is now

$$\mu^y(du, d\theta) \propto \exp(-\Phi(u; y))\mu_0(du|\theta)\pi_0(\theta)d\theta.$$

This is typically probed using a Metropolis-within-Gibbs algorithm that samples iteratively from the two conditional distributions:

1. (latent states given parameters and data)  $\mu^y(du|\theta) \propto \exp(-\Phi(u; y))\mu_0(du|\theta)$
2. (parameters given latent states)  $\mu^y(\theta|u) \propto \mu_0(du|\theta)\pi_0(\theta)$ ,

and it is an instance of what in Bayesian hierarchical models is commonly called a centred algorithm or equivalently a Metropolis-within-Gibbs algorithm based on a centred parameterisation of the model, see [13] for details and overview. Note that the sampling problem in (a) is precisely the one treated in Section 3. Note that in (b) only the prior structure matters for sampling the parameter.

It is well-documented that such component-wise updating schemes will mix poorly whenever the measures  $\mu_0(du|\theta)$ ,

for different  $\theta$ 's, are very different, say with large total variation distance for small perturbations of  $\theta$ . In fact, in many applications where  $X$  is infinite-dimensional these measures are mutually singular and the centred algorithm is reducible, i.e., it would never move from its initial values. A toy example is when  $\mu_0(du|\theta)$  is the law of a scaled Brownian motion  $\{\theta B_t\}_{t \in [0, T]}$ . Then given a sample  $(u(t), t \in [0, T])$ , its quadratic variation  $\langle u \rangle_t = \theta^2 t$  fully determines  $\theta$  up to sign, and so the family  $\{\mu_0(du|\theta)\}_{\theta > 0}$  is mutually singular.

A generic solution to this pathology is to work with a non-centred parameterisation of the hierarchical model, which is defined to be one under which a transformed latent state and the parameters are a priori independent. The Metropolis-within-Gibbs algorithm that targets the corresponding posterior is termed non-centred algorithm. The motivation behind this parameterisation, especially for infinite-dimensional models, is the following: if the data are not infinitely informative about  $u$ , hence a likelihood function exists, sets that have probability 1 under the prior also do under the posterior; hence if under the prior latent states and parameters are not perfectly dependent they will also not be under the posterior and the non-centred algorithm will be ergodic.

The developments of the previous two sections readily provide non-centred parameterisations of the hierarchical Bayesian inverse problem since the Gaussian white noise latent state  $\xi \sim \nu_0$ , and parameters  $\theta$  defining the map  $u = T(\xi, \theta)$  are a priori independent. The likelihood thus depends on both  $\xi$  and  $\theta$  and the posterior takes the form

$$\nu^\gamma(d\xi, d\theta) \propto \exp(-\Phi(T(\xi, \theta); y)) \nu_0(d\xi) \pi_0(\theta) d\theta.$$

By working in variables  $(\xi, \theta)$  rather than  $(u, \theta)$  we completely avoid lack of robustness arising from mutual singularity, by applying Metropolis-within-Gibbs to the variables  $(\xi, \theta)$  rather than  $(u, \theta)$ . Furthermore, by sampling  $\nu^\gamma(d\xi|\theta)$  using a dimension robust sampler as in the previous section we construct an overall methodology which is dimension robust. The method is provided as pseudocode in Algorithm 3.

---

**Algorithm 3** Non-centred Preconditioned Crank-Nicolson Within Gibbs

---

- 1: Fix  $\beta \in (0, 1]$ . Choose initial state  $(\xi^{(0)}, \theta^{(0)}) \in \Xi$  and set  $k = 0$ .
- 2: **for**  $k = 0, \dots, K - 1$  **do**
- 3:   Propose  $\xi^{(k)} = (1 - \beta^2)^{\frac{1}{2}} \xi^{(k-1)} + \beta \zeta^{(k)}$ ,    $\zeta^{(k)} \sim N(0, C)$ .
- 4:   Set  $\xi^{(k+1)} = \xi^{(k)}$  with probability

$$\min \left\{ 1, \exp \left( \Phi(T(\xi^{(k)}, \theta^{(k)}); y) - \Phi(T(\xi^{(k+1)}, \theta^{(k)}); y) \right) \right\}$$

or else set  $\xi^{(k+1)} = \xi^{(k)}$ .

- 5:   Propose  $\hat{\theta}^{(k)} \sim q(\theta^{(k)}, \cdot)$ .
- 6:   Set  $\theta^{(k+1)} = \hat{\theta}^{(k)}$  with probability

$$\min \left\{ 1, \exp \left( \Phi(T(\xi^{(k+1)}, \theta^{(k)}); y) - \Phi(T(\xi^{(k+1)}, \hat{\theta}^{(k)}); y) \right) \frac{q(\hat{\theta}^{(k)}, \theta^{(k)})}{q(\theta^{(k)}, \hat{\theta}^{(k)})} \frac{\pi_0(\hat{\theta}^{(k)})}{\pi_0(\theta^{(k)})} \right\}$$

or else set  $\theta^{(k+1)} = \theta^{(k)}$ .

- 7: **end for**
  - 8: **return**  $\{T(\xi^{(k)}, \theta^{(k)})\}_{k=0}^K$ .
-



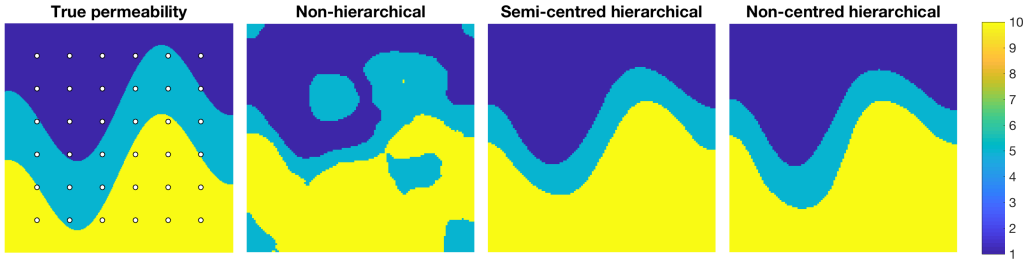


**FIGURE 3** The log-permeability that we wish to recover and the observation locations (left) and the conditional means from the three methods considered.

## 4.2 | Simulation experiments

We consider hierarchical level set priors for the problem of Example 1.3. The permeability field we aim to recover is shown in Figure 3, and the 36 points at which it is observed. Observations are corrupted by Gaussian white noise with standard deviation 0.05, resulting in an average relative error of 7.5%. We first consider a level set prior in which we threshold a Whittle-Matérn field at two levels. We then consider two hierarchical priors in which the length-scale parameter  $\tau$  of the underlying Gaussian field is treated as a hyperparameter, first using the hierarchical method introduced in [32], and then using a non-centred method as considered in this article. The method of [32] can be considered both centred, in that it maintains correlations between the field and hyperparameter under the prior, and non-centred, in that the likelihood is modified to explicitly depend on the hyperparameter in such a way that measure singularity issues are able to be circumvented. We will hence refer to this method as semi-centred. The data is generated using a uniform mesh of  $2^{18}$  points, and sampling is performed on a uniform mesh of  $2^{16}$  points. We generate  $2 \times 10^5$  samples, with the first  $5 \times 10^4$  discarded as burn-in when calculating means. For the non-hierarchical method the value  $\tau = 60$  is fixed, and for both hierarchical methods  $\tau$  is initialised at this value. The pushforwards of the corresponding three posterior means by the level set map are shown in Figure 3. That arising from the non-hierarchical method provides a fairly inaccurate reconstruction, due to the fixed length scale not matching that of the field to be recovered. Those arising from the hierarchical methods are similar to one another, both providing accurate reconstructions having learned appropriate length scales. In Figure 4 the trace of  $\tau$  is shown for both the semi- and non-centred hierarchical methods. The semi-centred chain takes approximately  $5 \times 10^4$  steps before  $\tau$  reaches the region of high posterior probability, whereas the non-centred chain takes approximately 200 steps. Additionally,  $\tau$  mixes worse with the semi-centred method. Thus, even though both methods are dimension-robust, the non-centred method provides much better statistical properties for approximately the same computational cost. Figure 4 also illustrates how well the parameter  $\tau$  is informed by the data, comparing the relatively flat prior density to the much more concentrated posterior density.

## 5 | GRAPH-BASED SEMI-SUPERVISED CLASSIFICATION

We illustrate the potential for uncertainty quantification in graph based learning within the context of the MNIST data set; see [35] and references therein. Further numerical results for this problem may be found in the appendix, as well as a second case study arising from medical imaging.

The MNIST dataset comprises 70000 images, of which 60000 are typically used for training, and 10000 for testing. In

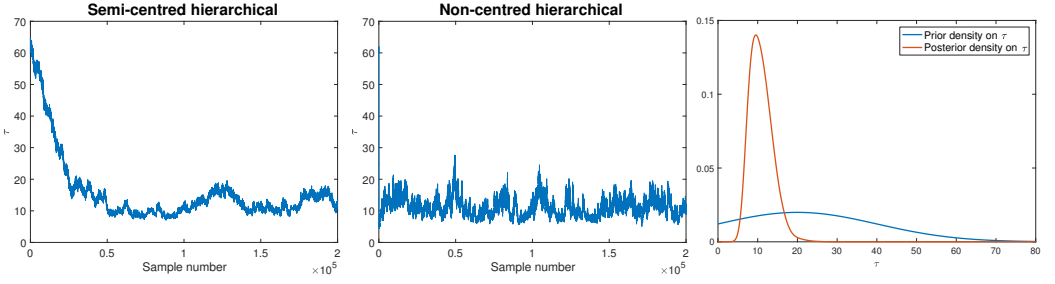


**FIGURE 4** The trace of the level-set parameter when using the semi-centred hierarchical method (left) versus the non-centred method (middle). The parameter takes approximately 250 times longer to burn-in with the semi-centred method, whilst also exhibiting poorer mixing. A comparison of the prior and posterior density on the length-scale parameter  $\tau$  for the non-centred hierarchical model is also shown (right). The mean has shifted and the variance significantly decreased, suggesting a high degree of identifiability of the parameter.

contrast to this supervised setup wherein the number of images with labels is of the same order of magnitude as the total number of images, we consider the semi-supervised setup in which the labels are sparse. Specifically, we initially use a training set of 200 images, so that the training set is 2% of the size of the test set as opposed to 600%. We then study human-in-the-loop learning, increasing the size of the training set, based on uncertainty quantification, to reduce the posterior uncertainty.

We therefore aim to classify  $N = 10200$  images. Each image is a  $20 \times 20$  greyscale representation of a handwritten digit 0-9 with pixel intensities in  $\{0, \dots, 255\}$ . We reshape and rescale these so that each datapoint  $x_j$  is a vector in  $[0, 1]^{400}$ . Additionally, as in [17] we project the datapoints onto their first  $d = 50$  principal components.

As we wish to perform multi-class classification, we use a discrete version of the vector level set method described in subsection 3.2.4, utilizing the same thresholding function

$$(Sv)(x) = e^{r(x;v)}, \quad r(x;v) = \arg \max_{r=1,\dots,10} v_r(x),$$

so that the unknown  $v : \mathbb{R}^N \rightarrow \mathbb{R}^{10}$  is a vector field defined on the set of datapoints. We will identify each component  $v_r : \mathbb{R}^N \rightarrow \mathbb{R}$  of  $v$  with a vector  $v_r \in \mathbb{R}^N$  in the natural way.

Our prior distribution on each  $v_r$  is chosen to be Gaussian with a Whittle-Matérn-type covariance operator based on a graph Laplacian in place of the continuum Laplacian. We construct a graph with  $N$  vertices  $\{x_j\}_{j=1}^N$ , and edge weights  $\{w_{ij}\}_{i,j=1}^N$  given by some similarity function  $w_{ij} = \eta(x_i, x_j)$  of the datapoints. Specifically let the weights be defined as the self-tuning weights introduced in [36]. Define  $L \in \mathbb{R}^{N \times N}$  to be the symmetric normalised graph Laplacian associated with this graph, i.e.  $L = I - D^{-\frac{1}{2}} W D^{-\frac{1}{2}}$  where  $W_{ij} = w_{ij}$  and  $D = \text{diag}_i(\sum_{j=1}^N w_{ij})$ . The eigenvectors and eigenvalues of this matrix contain a priori clustering information about the datapoints; see [2] and references therein.

Let  $\{\lambda_j\}_{j=0}^N$  denote the (non-negative) eigenvalues of  $L$ , ordered increasing, and denote  $\{q_j\}_{j=0}^N$  its corresponding eigenvectors. Given  $\alpha > 0$  and  $M \in \mathbb{N}$  with  $M \leq N$ , the random variable

$$\sum_{j=0}^M \frac{1}{(1 + \lambda_j)^{\alpha/2}} \xi_j q_j, \quad \xi_j \sim N(0, 1) \text{ i.i.d.}$$

has law  $N(0, C(\alpha, M))$ , where  $C(\alpha, M) = P_M(I + L)^{-\alpha} P_M^*$ , and  $P_M$  denotes the projection onto the span of the eigen-

vectors  $\{q_j\}_{j=0}^M$ ; the above sum is analogous to the Karhunen-Loève expansion. We use this as a prior distribution for each component  $v_r$  of the unknown vector field, assuming in addition that these components are mutually independent under the prior, so that given  $\alpha, M$ , the prior on  $v : \mathbb{R}^N \rightarrow \mathbb{R}^{10}$  is given by

$$\mu_0(v|\alpha, M) = N(0, C(\alpha, M) \oplus \dots \oplus C(\alpha, M)).$$

We treat the parameters  $\alpha, M$  hierarchically. A length-scale parameter could also be introduced and treated hierarchically, however we found empirically that this led to a lower classification accuracy in the mean. A non-hierarchical Bayesian approach to semi-supervised learning with this dataset was considered in [17]. There the prior covariance was fixed as  $C = L^{-1}$ , working on the orthogonal complement of  $q_0$  so that the inverse is well-defined, and binary classification was considered on subsets of images of two digits. We shift  $L$  by the identity to provide invertibility on the entirety of  $\mathbb{R}^N$ , increasing the flexibility of the prior.

Note that if the data points were uniformly distributed in a domain  $D \subset \mathbb{R}^d$ , then  $L$  could be viewed as an approximation of the continuum Laplacian operator on  $D$  [2], so that each component of the above prior can be viewed as an approximation to a Whittle-Matérn distribution on  $D$  per the SPDE characterisation (5). In practice the data will not be uniformly distributed, leading instead to an approximation to a non-isotropic Whittle-Matérn prior with a more general differential operator in place of the Laplacian.

We place uniform priors  $U(1, 100)$  and  $U(\{1, 2, \dots, 100\})$  on the hyperparameters  $\alpha$  and  $M$  respectively. The choice of prior on  $\alpha$  is made to be generally uninformative and not provide significant restriction. The choice of prior on  $M$  with  $M \ll N$  is made as a form of regularisation: higher order eigenvectors can contain a lot of noise in practice, reflecting outliers in the data, are not representative of eigenvectors in the large-data limit, and can lead to poor quality classification if included. Additionally it should be noted that if graph weights are able to distinguish between classes so that the graph has 10 connected components, the first 10 eigenvectors will contain information about the 10 classes. In practice the weights will not have this property, but they will still provide some distinction between classes, suggesting that there is little loss in neglecting the highest index eigenvectors.

We use the Bayesian level set method, and so the likelihood is given by

$$\Phi(v; y) = \frac{1}{2\gamma^2} \sum_{j=1}^J |(Sv)(x_j) - y_j|^2$$

where the  $y_j \in \{e^1, \dots, e^{10}\}$  are one-hot encodings of the labels. We assume that the accuracy of the labels is high; specifically we choose  $\gamma = 10^{-4}$ . With such a choice of  $\gamma$  there is little difference between using this or the probit likelihood function; indeed the resulting posteriors from both choices converge weakly to the conditioned measure

$$\mu(dv) \propto 1(\{(Sv)(x_j) = y_j \text{ for all } j = 1, \dots, J\})\mu_0(dv)$$

in the limit  $\gamma \rightarrow 0$  [37].

We apply the non-centred pCN-within-Gibbs algorithm, using random walk proposals for the hyperparameters, to generate 70000 samples. The first 20000 samples are discarded when calculating means. We introduce the measure of uncertainty associated with a data point  $x_j$  as

$$U(x_j) = 1 - \frac{10}{9} \|\mathbb{E}(Su)(x_j) - c\|_2^2$$



**FIGURE 5** The 20 most uncertain images (top) and a selection of 20 of the most certain images (bottom) under the posterior after labelling 200 images.

where  $c = \frac{1}{10} \sum_{r=1}^{10} e^r = (1/10, \dots, 1/10)$  is the centre of the simplex spanned by the classes. This is analogous to the variance of the classification in the case of binary classification as used in [17]; it is minimised when  $\mathbb{E}(Su)(x_j) = e^r$  for some  $r$ , and maximized when  $\mathbb{E}(Su)(x_j) = c$ . The normalising factor ensures  $U(x_j) \in [0, 1]$  for all  $x_j$ .

The mean value of the uncertainty across all 10200 images is 0.135. In Figure 5 we show the 20 images with the highest uncertainty value, as well as a selection of 20 images with zero uncertainty value, after labelling 200 images. On the whole, the certain images appear clearer and more ‘standard’ than the uncertain images, as would be expected. The uncertain images depict digits that have properties such as being sloped, cut off, or visually similar to different digits.

We can use this uncertainty measure to select an additional subset of the images to label, in an effort to decrease overall uncertainty in the classification. We now provide labels for the 100 most uncertain images, in addition to the original 200 images, and perform the MCMC simulations again. This could be interpreted as a form of human-in-the-loop learning, wherein an expert provides labels for data points deemed most uncertain by the algorithm. This reduces the mean uncertainty across all images to 0.100. As a comparison, we also consider labeling an additional set of the 100 most certain points rather than most the uncertain points, that is, points with  $U(x_j) = 0$ ; this has a lesser impact, reducing the mean uncertainty to 0.128.

## 6 | CONCLUSIONS

The aim of this paper has been threefold. First, to introduce a plug-and-play MCMC sampling framework for posterior inference in Bayesian inverse problems with non-Gaussian priors. The user needs to specify the elements of the model and a white noise transformation. Second, to demonstrate the success of the approach in challenging problems where we showcase the desired robustness with respect to the dimension of the latent process, the advantages of the method over alternative plug-and-play methods, such as random walk Metropolis algorithms, and its comparable performance to tailored methods in models where such are available. Third, to showcase the wide range of applications that this methodology is appropriate for. The generality of the approach makes it difficult to develop a unifying theoretical basis that establishes the observed robustness and the dimension-independent scaling of the algorithms. We believe, however, that the power of the examples of the methodology given here will act as impetus for the development of such a theory.

**Acknowledgements** The authors are grateful for helpful discussions with Andrea Bertozzi, who suggested the human-in-the-loop approach in section 5. MMD and AMS are supported by AFOSR Grant FA9550-17-1-0185 and ONR Grant N00014-17-1-2079.

## REFERENCES

- [1] Lovász L. Large networks and graph limits, vol. 60. American Mathematical Society Providence; 2012.

- [2] García Trillos N, Slepčev D. A variational approach to the consistency of spectral clustering. *Applied and Computational Harmonic Analysis* 2016;.
- [3] Trillos NG, Kaplan Z, Samakhoana T, Sanz-Alonso D. On the Consistency of Graph-based Bayesian Learning and the Scalability of Sampling Algorithms. *arXiv preprint arXiv:171007702* 2017;.
- [4] Cotter SL, Roberts GO, Stuart AM, White D, et al. MCMC methods for functions: modifying old algorithms to make them faster. *Statistical Science* 2013;28(3):424–446.
- [5] Beskos A, Girolami M, Lan S, Farrell PE, Stuart AM. Geometric MCMC for Infinite-Dimensional Inverse Problems. *Journal of Computational Physics* 2017;335:327–351.
- [6] Cui T, Law KJ, Marzouk YM. Dimension-independent likelihood-informed MCMC. *Journal of Computational Physics* 2016;304:109–137.
- [7] Law KJ. Proposals which speed up function-space MCMC. *Journal of Computational and Applied Mathematics* 2014;262:127–138.
- [8] Titsias MK, Papaspiliopoulos O. Auxiliary gradient-based sampling algorithms. *Journal of the Royal Statistical Society series B* 2018;to appear.
- [9] Lassas M, Saksman E, Siltanen S. Discretization-invariant Bayesian inversion and Besov space priors. *Inverse Problems and Imaging* 2009;3(1):87–122. <http://aimsciences.org/journals/displayArticlesnew.jsp?paperID=3965>.
- [10] Markkanen M, Roininen L, Huttunen JM, Lasanen S. Cauchy difference priors for edge-preserving Bayesian inversion with an application to X-ray tomography. *arXiv preprint arXiv:160306135* 2016;.
- [11] Sullivan T. Well-posed Bayesian inverse problems and heavy-tailed stable quasi-Banach space priors. *arXiv preprint arXiv:160505898* 2016;.
- [12] Knapik B, Szabó B, van der Vaart A, van Zanten J. Bayes procedures for adaptive inference in inverse problems for the white noise model. *Probability Theory and Related Fields* 2016;164(3-4):771–813.
- [13] Papaspiliopoulos O, Roberts GO, Sköld M. A general framework for the parametrization of hierarchical models. *Statistical Science* 2007;p. 59–73.
- [14] Agapiou S, Bardsley JM, Papaspiliopoulos O, Stuart AM. Analysis of the Gibbs sampler for hierarchical inverse problems. *SIAM/ASA Journal on Uncertainty Quantification* 2014;2(1):511–544.
- [15] Wang Z, Bardsley JM, Solonen A, Cui T, Marzouk YM. Bayesian inverse problems with l1 priors: a randomize-then-optimize approach. *SIAM Journal on Scientific Computing* 2017;in press.
- [16] Wahba G. Spline models for observational data. *SIAM*; 1990.
- [17] Bertozzi AL, Luo X, Stuart AM, Zygalakis KC. Uncertainty Quantification in the Classification of High Dimensional Data. *SIAM J Uncertainty Quantification*, to appear 2018;.
- [18] Dashti M, Stuart AM. The Bayesian approach to inverse problems. *Handbook of Uncertainty Quantification* 2017;.
- [19] Rasmussen CE, Williams CK. Gaussian processes for machine learning. the MIT Press 2006;2(3):4.
- [20] Lindgren F, Rue H, Lindström J. An explicit link between Gaussian fields and Gaussian Markov random fields: the stochastic partial differential equation approach. *Journal of the Royal Statistical Society Series B: Statistical Methodology* 2011;73(4):423–498. <http://dx.doi.org/10.1111/j.1467-9868.2011.00777.x>.
- [21] Rue H, Held L. Gaussian Markov random fields: theory and applications. *Chapman & Hall*; 2005.

- [22] Roininen L, Huttunen JM, Lasanen S. Whittle-Matérn priors for Bayesian statistical inversion with applications in electrical impedance tomography. *Inverse Problems Imaging* 2014;8(2):561–586.
- [23] Daon Y, Stadler G. Mitigating the Influence of the Boundary on PDE-based Covariance Operators. *arXiv preprint arXiv:161005280* 2016;.
- [24] Hosseini B. Well-posed Bayesian Inverse Problems with Infinitely-Divisible and Heavy-Tailed Prior Measures. *arXiv preprint arXiv:160907532* 2016;.
- [25] Dashti M, Harris S, Stuart AM. Besov priors for Bayesian inverse problems. *Inverse Problems and Imaging* 2012;6:183–200.
- [26] Agapiou S, Burger M, Dashti M, Helin T. Sparsity-promoting and edge-preserving maximum a posteriori estimators in non-parametric Bayesian inverse problems. *arXiv preprint arXiv:170503286* 2017;.
- [27] Nardon M, Pianca P. Simulation techniques for generalized Gaussian densities. *Journal of Statistical Computation and Simulation* 2009;79(11):1317–1329.
- [28] Chambers JM, Mallows CL, Stuck B. A method for simulating stable random variables. *Journal of the american statistical association* 1976;71(354):340–344.
- [29] Osher S, Sethian JA. Fronts propagating with curvature dependent speed: algorithms based on Hamilton-Jacobi formulations. *Journal of Computational Physics* 1988;79:12–49.
- [30] Santosa F. A level-set approach for inverse problems involving obstacles. *ESAIM* 1996;1(January):17–33.
- [31] Iglesias M, Lu Y, Stuart AM. A Bayesian level set method for geometric inverse problems. *Interfaces and Free Boundaries* 2016;18:181–217.
- [32] Dunlop MM, Iglesias MA, Stuart AM. Hierarchical Bayesian level set inversion. *Statistics and Computing* 2016;.
- [33] Hu H, Sunu J, Bertozzi A. Multi-class graph Mumford-Shah model for plume detection using the MBO scheme. *Lecture Notes in Computer Science (including subseries Lecture Notes in Artificial Intelligence and Lecture Notes in Bioinformatics)* 2015;8932.
- [34] Vollmer SJ. Dimension-independent MCMC sampling for inverse problems with non-Gaussian priors. *SIAM/ASA Journal on Uncertainty Quantification* 2015;3(1):535–561.
- [35] LeCun Y, Bottou L, Bengio Y, Haffner P. Gradient-based learning applied to document recognition. *Proceedings of the IEEE* 1998;86(11):2278–2324.
- [36] Zelnik-Manor L, Perona P. Self-tuning spectral clustering. In: *Advances in neural information processing systems*; 2005. p. 1601–1608.
- [37] Dunlop MM, Slepčev D, Stuart AM, Thorpe M. Large data and zero noise limits of graph-based semi-supervised learning algorithms. In preparation 2018;.
- [38] Somersalo E, Cheney M, Isaacson D. Existence and uniqueness for electrode models for electric current computed tomography. *SIAM Journal on Applied Mathematics* 1992;52(4):1023–1040.
- [39] Dunlop MM, Stuart AM. The Bayesian formulation of EIT: analysis and algorithms. *Inverse Problems and Imaging* 2016;10:1007–1036.
- [40] Roininen L, Girolami M, Lasanen S, Markkanen M. Hyperpriors for Matérn fields with applications in Bayesian inversion. *arXiv preprint arXiv:161202989* 2016;.
- [41] Dunlop MM, Girolami M, Stuart AM, Teckentrup AL. How deep are Deep Gaussian Processes?; 2017, submitted.
- [42] Adler A, Lionheart WR. Uses and abuses of EIDORS: an extensible software base for EIT. *Physiological measurement* 2006;27(5):S25.

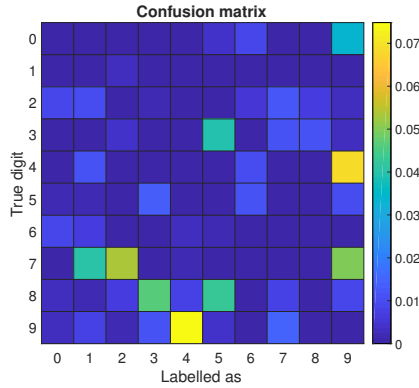


**FIGURE 6** The confusion matrix arising from the MNIST simulations in section 5 of the article.

## A | APPENDIX: ADDITIONAL ILLUSTRATIONS

### A.1 | Graph-Based Semi-Supervised Classification

We provide some additional details regarding the simulations in section 5 of the article. In Figure 6 we show the confusion matrix arising from the classification with the initial 200 labels. The  $(i, j)$ th entry of this matrix represents the percentage of images of digit  $i$  that have been classified as digit  $j$ ; we set the diagonal to zero to emphasise contrast between the off-diagonal entries. The most misclassified pairs are those digits that can look most similar to one another, such as 4 and 9, or 3 and 8.

In Figure 7 we show how the distribution of uncertainty changes when we perform the human-in-the-loop process iteratively, both for the most uncertain and most certain images. When the most uncertain images are labelled, the number of images in the bin of lowest uncertainty increases significantly. In particular, the first labelling of 100 additional images increases its size by over 1000. After labelling 300 additional images, the mean uncertainty has reduced to 0.070. On the other hand, we see that labelling the most certain images does not change the distribution of uncertainty as much, and the mean uncertainty has become 0.132 after labelling an additional 300 images.

### A.2 | Medical Imaging

We provide an example of a more exotic prior, and its application to the solution of a nonlinear inverse problem. Specifically we consider the EIT problem, and use a Matérn-type prior with a spatially varying length-scale field that is to be jointly inferred.

#### A.2.1 | Problem Setup

We consider the Electrical Impedance Tomography (EIT) problem of recovering the interior conductivity of a body from current measurements on its boundary. Mathematically the model is similar to Example 1.3, except measurements are made at the boundary for a variety of different boundary conditions, rather than in the interior. Full details of the model are given in [38], and details of the Bayesian approach are provided in [39]. We focus on the task of recovering a binary conductivity with two distinct length scales associated with it.

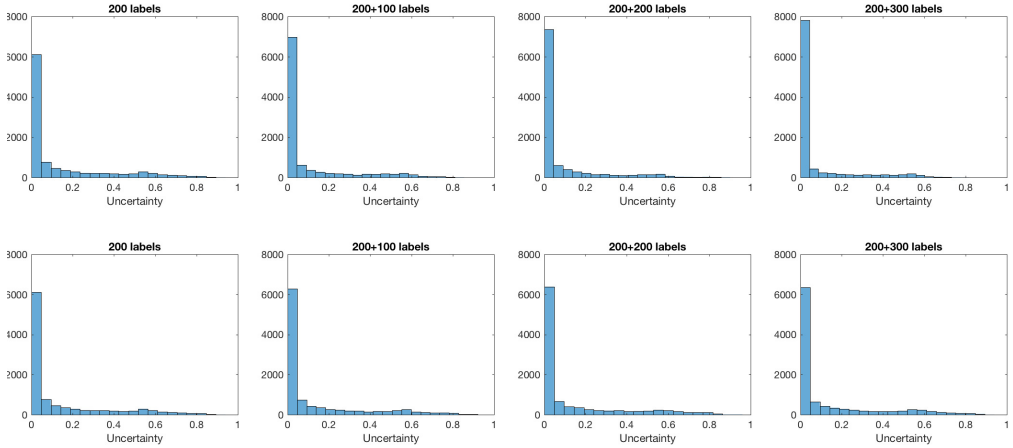


**FIGURE 7** Histograms illustrating the distribution of uncertainty across images as the number of labelled datapoints is increased using human-in-the-loop learning, iteratively labelling the most uncertain points (top) and most certain points (bottom).

## A.2.2 | Prior

If we were to use a thresholded hierarchical Whittle-Matérn distribution as the prior, as in subsection 4.2 of the article, then the assertion of a constant length-scale throughout the body would restrict reconstruction accuracy. For our prior we hence assume in addition that the hyperprior on the length-scale is itself a thresholded Whittle-Matérn distribution with a fixed length-scale; such anisotropic length-scales make sense from the SPDE characterisation (5) of the distributions. Such priors have been considered without thresholding in [40]. The Metropolis-within-Gibbs algorithm introduced in the main article, Algorithm 3, assumes existence of a Lebesgue density of the hyperparameter. This is not the case here, though the methodology readily extends; see [41] for an explicit statement of the algorithm used.

## A.2.3 | Likelihood

We take the true conductivity to be a draw from the prior, so that we may also examine the ability to recover the length-scale field. Observations are perturbed by white Gaussian noise with standard deviation 0.002, leading to a large median relative error of approximately 21%. In Figure 8 we show the true conductivity field we wish to recover, its length-scale field, and the observed data.

## A.2.4 | Posterior

Samples are generated on the square  $(-1, 1)^2$  and restricted to the domain  $D = B_1(0)$ ; this allows for some boundary effects to be ameliorated – see [22, 23] for further discussion regarding boundary effects of this class of Gaussian random fields. Each field is sampled on a uniform mesh of  $2^8 \times 2^8$  points so that there are  $2^{17}$  unknowns in total. The forward model is evaluated with a finite element method using the EIDORS software [42] on a mesh of 46656 elements,



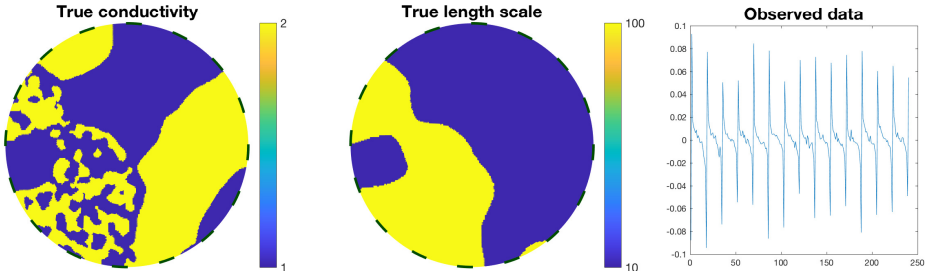


**FIGURE 8** The true conductivity field (left), its associated length-scale field (middle), and the noisy data generated from this (right).

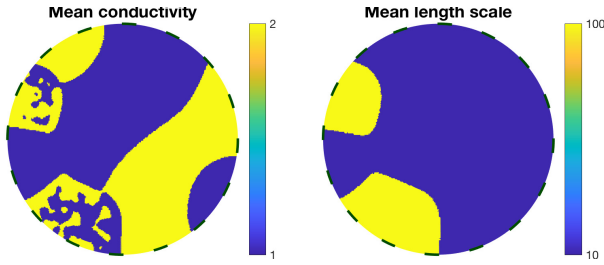


**FIGURE 9** The pushforwards of the sample mean of the conductivity field (left) and length-scale field (right).

with spline interpolation used to move from the sampling mesh.

We generate  $4 \times 10^5$  samples using the non-centred pCN within Gibbs method. The pCN method may be used to update both fields simultaneously, however we found in practice that a Metropolis-within-Gibbs method led to better mixing. The pushforward of the sample mean by the thresholding maps are shown in Figure 9; the first  $1 \times 10^5$  samples are discarded as burn-in in the calculation of these. The main features of the conductivity are recovered, and some information about the shape of the length-scale field is evidently contained within the data. The recovery of both fields is more accurate near to the boundary than the centre of the domain, as is to be expected from the nature of the measurements. Finally in Figure 10 we show some representative samples of the conductivity field, and observe that they share qualitative properties with the true conductivity.

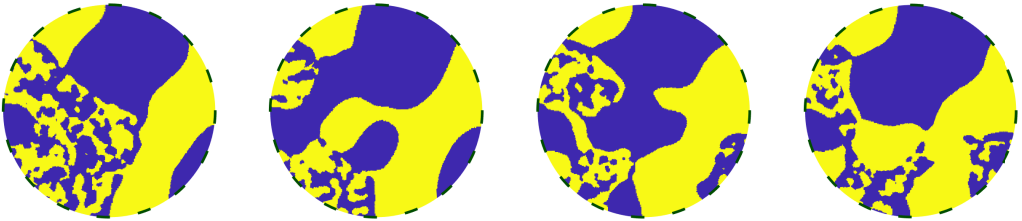


**FIGURE 10** A collection of representative samples of the conductivity field of the chain, after a burn-in period.